copy. The transmission data yielded an average dichroic ratio (R) of 2 at 490 nm, where R is the ratio of absorbance parallel to versus perpendicular to the film (*20*). The conductivity of the multiwire cables in the concentrated 10^{-2} M nanocomposite was determined by an optical method because the material exhibits a high contact resistance. We estimated the conductivity from the plasma resonance (ω_p) exhibited by $(LiMo_3Se_3)_n$ in the infrared region (*10*). The infrared spectrum of a 10^{-2} M poly(VC)-$(LiMo_3Se_3)_n$ gel sheared between two KBr disks displays a broad $(LiMo_3Se_3)_n$ plasma absorption centered at ~1100 cm^{-1}. Fitting the absorption according to a Drude model (*21*) gives ω_p and an estimated conductivity σ of 10^2 to 10^3 S cm^{-1} from $\sigma = \omega_p^2\tau/4\pi$, where τ is the carrier relaxation time. This compares favorably with a conductivity of 2×10^2 S cm^{-1} measured for a neat $(LiMo_3Se_3)_n$ thin film (*10*).

REFERENCES AND NOTES

1. G. M. Whitesides and J. P. Mathius, *Science* **254**, 1312 (1991); J. M. Lehn, *Angew. Chem. Int. Ed. Engl.* **29**, 1304 (1990); C. Carter, *Molecular Electronic Devices* (Dekker, New York, 1982).
2. G. Wegner *et al.*, *Mater. Res. Soc. Symp. Proc.* **328**, 15 (1994).
3. L. A. Bumm *et al.*, *Science* **271**, 1705 (1996).
4. T. M. Whitney, J. S. Jiang, P. C. Searson, C. C. Chien, *ibid.*, **261**, 1316 (1993); C. A. Huber *et al.*, *ibid.* **263**, 800 (1994).
5. R. W. Wagner and J. S. Lindsey, *J. Am. Chem. Soc.* **116**, 9759 (1994).
6. C. F. van Nostrum, S. J. Picken, R. J. M. Nolte, *Angew. Chem. Int. Ed. Engl.* **33**, 2173 (1994).
7. P. M. Ajayan, O. Stephan, C. Colliex, D. Trauth, *Science* **265**, 1212 (1994); H. Hoshino, T. Ito, N. Donkai, H. Urakawa, K. Kajiwara, *Polym. Bull.* **29**, 453 (1992).
8. J. H. Golden, H. Deng, F. J. DiSalvo, J. M. J. Fréchet, P. M. Thompson, *Science* **268**, 1463 (1995).
9. P. J. Flory, *Macromolecules* **11**, 1138 (1978).
10. J. M. Tarascon *et al.*, *J. Solid State Chem.* **58**, 290 (1985); J. H. Golden, F. J. DiSalvo, J. M. J. Fréchet, *Chem. Mater.* **7**, 232 (1995).
11. M. Potel *et al.*, *J. Solid State Chem.* **35**, 286 (1980).
12. R. Chevrel, M. Sergent, J. Prigent, *ibid.* **3**, 515 (1971).
13. Viscometric analysis of both neat poly(VC) and the poly(VC) nanocomposite yielded a chromatogram displaying a bimodal distribution and a molecular weight of ~10^6 as compared to a molecular weight of 3×10^6 for a poly(styrene) standard. Differential scanning calorimetry (DSC) from 50° to 450°C (5°C min^{-1}) revealed a broad endotherm commencing at 240°C and centered at 311°C. The polymer used for gel permeation chromatography and DSC analysis was precipitated twice from dimethyl formamide into acetone and then dried in vacuo.
14. M. L. Kaplan, E. A. Reitman, R. J. Cava, L. K. Holt, E. A. Chandross, *Solid State Ionics* **25**, 37 (1987).
15. S. J. Pennycook and L. J. Boatner, *Nature* **336**, 565 (1988). We obtained the STEM images using a Vacuum Generators HB-501A STEM at 100 keV equipped with an analytical pole piece (C_S = 3.3 mm), where C_S is the spherical aberration coefficient at a working vacuum of ~10^{-10} torr. The theoretical resolution limit is 2.7 Å.
16. J. Wu, G. Lieser, G. Wegner, *Adv. Mater.* **8**, 151 (1996).
17. L. D. Landau and E. M. Lifshitz, *Theory of Elasticity* (Pergamon, New York, 1970), p. 75.
18. C. Herring and J. K. Galt, *Phys. Rev. Ser. 2* **85**, 1060 (1952).
19. Scanning electron micrograph microprobe samples were prepared in an argon-filled inert-atmosphere box and loaded for analysis with a minimum of air exposure (<30 s). We conducted the analyses using a JEOL 733 microprobe at 15 keV.
20. We acquired polarized ultraviolet-visible transmission spectra using a J. A. Woolam spectroscopic ellipsometer. Spectra were taken from 300 to 840 nm, in 7-nm increments, with the polarizer set either parallel to or perpendicular to the shearing direction of the glass slide.
21. N. W. Ashcroft and N. D. Mermin, *Solid State Physics* (Holt, Rinehart, and Winston, New York, 1976), pp. 16–20.

22. This research was supported by the Materials Research Laboratory Program of the National Science Foundation under award DMR-9121654.

8 April 1996; accepted 29 May 1996

Visualization of Slow Axonal Transport in Vivo

Sumio Terada, Takao Nakata, Alan C. Peterson, Nobutaka Hirokawa*

In axons, cytoskeletal constituents move by slow transport. However, it remains controversial whether axonal neurofilaments are dynamic structures in which only subunits are transported or whether filaments assemble in the proximal axon and are transported intact as polymers to the axon terminus. To investigate the form neurofilament proteins take during transport, neurons of transgenic mice lacking axonal neurofilaments were infected with a recombinant adenoviral vector encoding epitope-tagged neurofilament M. Confocal and electron microscopy revealed that the virally encoded neurofilament M was transported in unpolymerized form along axonal microtubules. Thus, neurofilament proteins are probably transported as subunits or small oligomers along microtubules, which are major routes for slow axonal transport.

Neurons are highly asymmetric cells. Their axonal processes can extend for an exceptionally long distance, but there is a complete lack of protein synthesis machinery in axons. Thus, all materials necessary for axonal maintenance and function are transported from the cell body by fast and slow transport mechanisms. Components of the neuronal cytoskeleton and several axonal cytoplasmic proteins are conveyed by slow axonal transport at a rate of 0.1 to 3 mm/day (*1*). Although the process has been analyzed by various methods, it still remains controversial whether axonal neurofilaments are dynamic structures in which only subunits are transported (*2*, *3*) or whether the axonal neurofilament cytoskeleton polymerizes in the cell body immediately after synthesis and subsequently is transported as a coherent column to the axon terminus by a sliding mechanism (*4*, *5*).

To study the mechanisms involved in slow axonal transport, we constructed a recombinant adenoviral vector (*6*) encoding an epitope-tagged neurofilament M protein. The rat gene encoding neurofilament M (*7*) was modified by polymerase chain reaction techniques to encode a c-Myc epitope tag (*8*). Because the COOH-terminus of neurofilament M is only poorly conserved among species (*9*), the precise amino acid sequence is unlikely to be critical, and we introduced the c-Myc epitope in that domain. The neurofilament M protein by itself cannot form 10-nm filaments (*10*, *11*), which precludes any direct evaluation of functional consequences arising from this modification. However, in a baculovirus expression system, neurofilament M can form 10-nm filaments by copolymerizing with neurofilament L. Epitope tagging did not lead to any observable changes in cross-bridge formation, spacing between core filaments, or core filament assembly in this expression system (*11*). The recombinant adenovirus encoding the epitope-tagged rat neurofilament M protein (AxCA-NT-NFMmyc) was constructed by homologous recombination between the expression cosmid cassette and the parental virus genome (*12*). This vector was then used to infect the fourth lumbar (L4) dorsal root ganglion (DRG) neurons of both normal and transgenic mice (*13*). In line 44A transgenic mice, expression of an NF-H–β-galactosidase fusion protein causes the entire intermediate filament cytoskeleton to precipitate in the cell body, and consequently axons lack a neurofilament cytoskeleton (*14*). As neurofilament M proteins cannot by themselves form polymers (*10*, *11*),

S. Terada, Institute for Brain Research, Faculty of Medicine, University of Tokyo, 7-3-1 Hongo, Bunkyo-ku, Tokyo 113, Japan.
T. Nakata, Department of Anatomy and Cell Biology, Faculty of Medicine, University of Tokyo, 7-3-1 Hongo, Bunkyo-ku, Tokyo 113, Japan.
A. C. Peterson, Molecular Oncology Group, McGill University, H5-35, 687 Pine Avenue West, Montreal, Quebec H3A 1A1, Canada.
N. Hirokawa, Institute for Brain Research and Department of Anatomy and Cell Biology, Faculty of Medicine, University of Tokyo, 7-3-1 Hongo, Bunkyo-ku, Tokyo 113, Japan.

*To whom correspondence should be addressed. E-mail: hirokawa@m.u-tokyo.ac.jp

investigation of the transport of the virally encoded gene product was expected to reveal whether unassembled neurofilament protein can be transported by slow axonal transport.

Copolymerization of the tagged neurofilament M protein into the endogenous intermediate filament network was observed in DRG neurons (Fig. 1). A stock of AxCA-NT-NFMmyc was concentrated (*15*) to 10^{10} to 10^{11} plaque-forming units (PFUs) per milliliter and injected into the left L4 DRG of line 44A transgenic mice. A characteristic filamentous distribution pattern of the Myc epitope was observed in the DRG cell bodies by epifluorescent microscopy (Fig. 1B). Coassembly of the Myc-tagged neurofilament M protein with endogenous 10-nm intermediate filaments was also revealed by immunoelectron microscopy (Fig. 1D). The neurofilaments precipitated in the neuronal cell bodies of line 44A mice assumed a tightly spaced parallel array. Ultrastructural analysis of the infected DRG cell bodies revealed a similar configuration of filaments, some of which were labeled with silver grains. When we compared them with noninfected cells, we did not detect any pathological changes of structural components (*16*) in DRG neurons infected with vector (Fig. 1D). The recombinant adenovirus vector had little or no cytotoxic effect on DRG neurons, even at the ultrastructural level.

At 5 or 7 days after infection, sciatic nerves and spinal roots were dissected, sectioned in the longitudinal plane, and analyzed by immunocytochemistry with the use of a monoclonal antibody (mAb) to c-Myc. Confocal laser scanning microscopy revealed that the tagged neurofilament protein was readily detectable in infected DRG cell bodies (Fig. 2). Also, it was transported into sciatic nerve

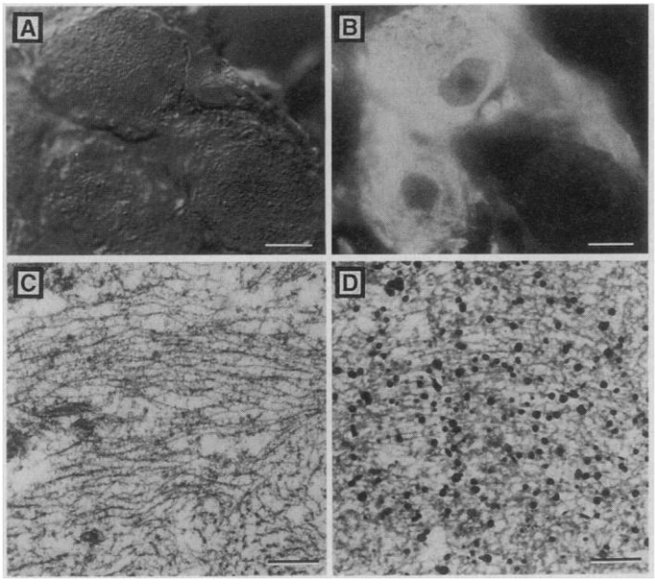

Fig. 1. Successful copolymerization of tagged neurofilament protein into 10-nm filaments in DRG neurons of line 44A transgenic mice infected with AxCA-NT-NFMmyc in vivo. (**A**) Differential interference contrast (DIC) image of a DRG infected with vector containing viruses. (**B**) Characteristic filamentous distribution pattern of transgene products as detected by epifluorescent microscopy in the same specimen as shown in (A). Two of three DRG neurons shown in the DIC image are infected with vectors. Scale bars in (A) and (B), 10 μm. (**C**) Cell body of a DRG neuron from a noninfected transgenic mouse, processed by conventional electron microscopic procedures. (**D**) Immunoelectron microscopic preparation of vector-infected DRG neurons from line 44A mice, showing close parallel arrays of filaments with silver grains, which are highly reminiscent of the neurofilament configuration typical of such cells. Tannic acid, instead of osmium tetroxide, was used for contrast enhancement. Scale bars in (C) and (D), 100 nm.

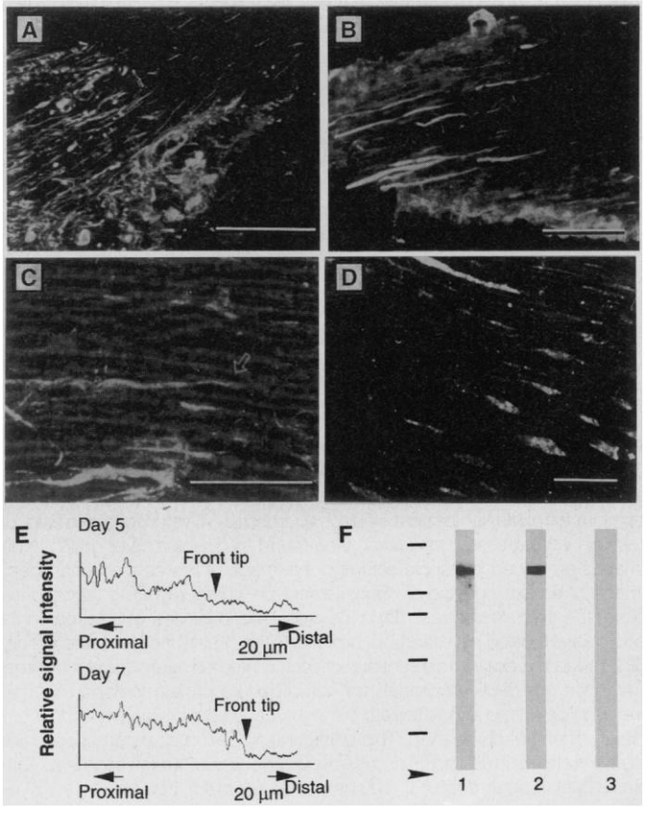

Fig. 2. Vector-encoded neurofilament-M protein detected by immunocytochemistry and immunoblotting in sciatic nerve axons. Highly concentrated AxCA-NT-NFMmyc was injected into L4 dorsal root ganglia of transgenic mice, and animals were killed 2, 5, or 7 days after infection. Sciatic nerves were dissected, sectioned in the longitudinal plane, and analyzed by immunocytochemistry with the use of a mAb to c-Myc. (**A** through **C**) show axons on day 5 after infection. (A) L4 DRG. Scale bar, 250 μm. (B) Section adjoining (A), distal portion. Scale bar, 100 μm. (C) The front tip of the positive staining, located about 5 mm from the DRG (arrow). Scale bar, 50 μm. We could distinguish the leading edge of fluorescence in a labeled axon from a case in which the labeled axon altered its course and moved above or below the plane of the tissue section by analyzing consecutive reconstructed cross-sectional images calculated with confocal laser scanning microscopy. (**D**) Day 7 after infection. The synchronous termination of transported transgene products in multiple axons, measured and confirmed in the same way as in (C), is shown. Scale bar, 25 μm. In (A) through (D), tagged neurofilament proteins are traveling in the axons toward the right. (**E**) Distribution of transgene product declines abruptly against the background. Upper panel, day 5 after infection [the same sample shown in (C)]; lower panel, day 7 after infection. The vertical axis shows relative signal intensity, measured by confocal laser scanning microscopy. The horizontal axis shows distance along the longitudinal axis of the stained axon. The locations of the front tips of positive staining are indicated by arrows. For immunoblotting, virus-injected animals were killed 2 days after infection and both proximal and distal nerve fragments within 2 mm distance from the DRG were isolated. (**F**) Lanes 1 and 2, samples from nerve fragments from a virus-injected DRG; lane 3, samples from contralateral nerve fragments from a negative control. Lanes 1 and 3 were blotted with mAb to c-Myc; lane 2 was blotted with antibody to neurofilament M. Bars on the left indicate molecular mass markers of 200, 116, 97, 66, and 45 kDa (from the top down), and the arrowhead shows the position of the dye front.

axons and in some, when analyzed by serial optical sectioning, labeled protein was continuously detectable from the DRG cell body to the leading edge of its transport (Fig. 2). To enhance antibody penetration in this experiment, we used only paraformaldehyde fixative. Successful staining was confirmed by analysis of confocal laser scanning microscope images in which reconstructed cross sections of axons showed uniform and continuous labeling. At 5 days after infection, the front tip was located about 5 mm from DRG neurons, and at 7 days it had traveled about 7 mm from the ganglion. These results are compatible with the transport speed of slow component a (SCa), which includes the endogenous neurofilament proteins (*4*). Furthermore, as shown in Fig. 2D, we often observed several leading edges of staining in one specimen. This indicates a very synchronous rate of transport in different axons. In addition, the distribution of vector-derived neurofilament M assessed by measurement of the signal intensity profile along the labeled axons revealed that the concentration of tagged neurofilament proteins was essentially uniform throughout the labeled region. At the leading edge, the signal declined abruptly, usually extinguishing in less than 70 μm (Fig. 2E). These results are consistent with the evidence from metabolic labeling studies for both direct transport of cytoskeletal proteins and the existence of a transport mechanism involving more than simple diffusion (*17*). We could not detect any labeling in Schwann cells; even in reconstituted cross-sectional images of nerve fibers, the fluorescence was detected only in axons, and the concentric circular or elliptic stainings that corresponded to the positions of the Schwann cell cytoplasm were never observed (*18*). We confirmed that the transgene products that moved into axons were intact tagged neurofilament M proteins, rather than tagged proteolytic fragments, by immunoblotting analysis (*19*); mAb to c-Myc detected a single band in axoplasm (Fig. 2F), which corresponded to the labeling by mAb to neurofilament M. There were no degraded fragments. Some of the tagged neurofilament M proteins were phosphorylated in cell bodies at this stage, whereas in axons, no phosphorylation of tagged proteins was observed (*20*). As neurofilament M proteins cannot form polymers by themselves (*10*, *11*) and most axons in these mice do not possess polymerized neurofilaments, it is likely that neurofilament proteins were transported as monomers or small oligomers.

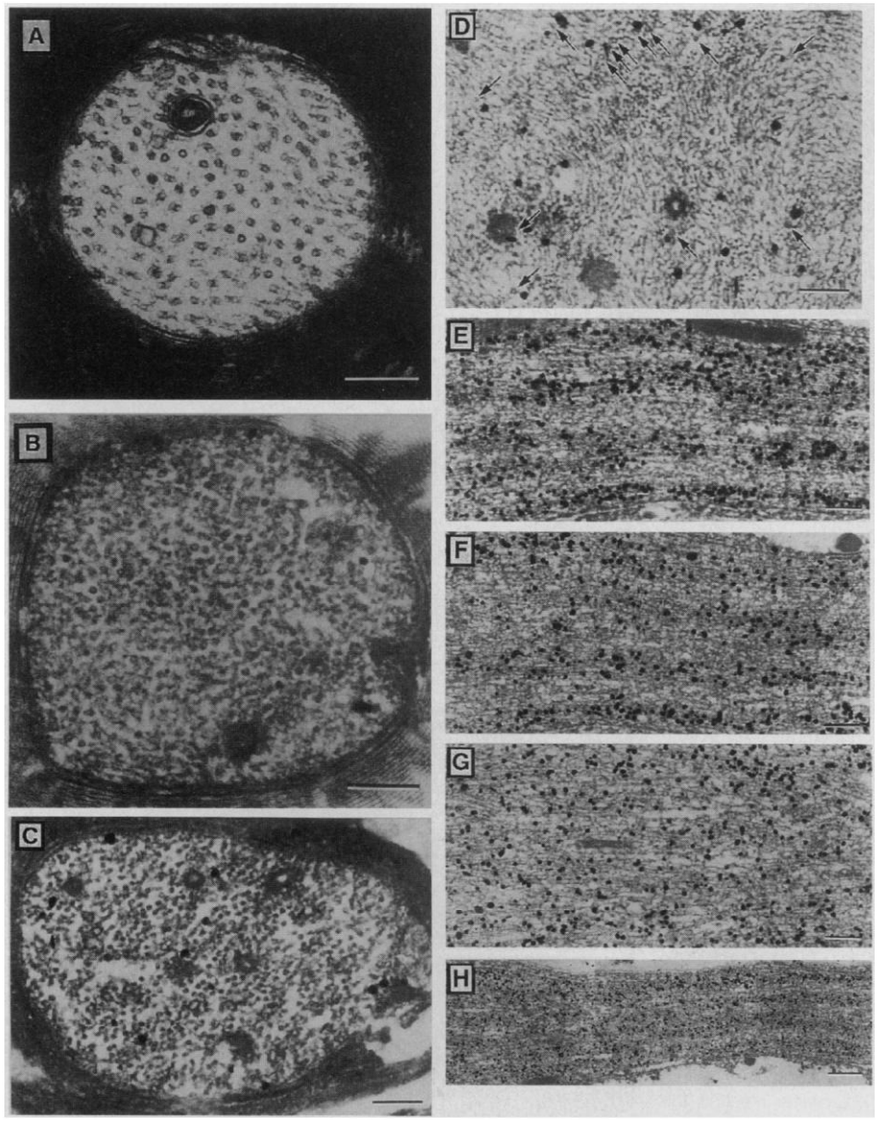

Fig. 3. Immunoelectron microscopic analysis of transported tagged neurofilament protein in sciatic nerve axons of line 44A transgenic mice. (**A**) and (**B**) are cross-sectional views of neurofilament polymer-free axons processed (A) by conventional electron microscopic procedures and (B) by tannic acid, instead of osmium tetroxide, for immunoelectron microscopy. [We used tannic acid for contrast enhancement in (B) through (H) because osmification was found to dissolve silver grains. Note the difference between the images enhanced by tannic acid and the image of the conventional specimen (A).] (**C**) Cross-sectional image of an axon devoid of neurofilament polymers, revealing tagged unpolymerized proteins traveling down the axon. In contrast, (**D**) is the cross-sectional view of an axon containing neurofilament polymers and shows labeled neurofilament proteins (silver grains) located preferentially along microtubules (arrows). (**E** through **H**) Longitudinal sections of vector-infected neurofilament polymer-positive axons, showing the existence of selective channels for neurofilament protein transport. Tagged neurofilament proteins are traveling down the axons toward the right. Labeled proteins were most often situated in a line along the longitudinal axis of the axon. This configuration becomes progressively more evident in the distal portion of axons shown in (E) and (F) and is obscured in proximal axon segments (G). (H) is at a lower magnification. Scale bars in (A) through (G), 100 nm; scale bar in (H), 500 nm.

It was not possible to perform longer term experiments with line 44A, because such mice have a normal immune system. The E2A product expressed by cells infected with the viral vector causes inflammation to develop after 7 days because of major histocompatibility complex–dependent cytotoxic T lymphocytes (*21*). Genetically athymic mice of the BALB/c-nu/nu strain lack a cellular immune response and do not mount an inflammation response, and so can be studied beyond 7 days after infection. In such mice, even at 2 weeks after infection, the distribution of transgene product followed the same pattern as in the line 44A experiments. The transport rate in such mice was similarly compatible with that of SCa components and, as in the neurofilament-deficient axons, the leading edge of labeling terminated abruptly (*20*).

To determine the subcellular distribution of the transported, tagged neurofilament pro-

tein and to confirm that it could be transported in axons free of endogenous neurofilament polymer, we carried out immunoelectron microscopic analysis of neurons 3 days after infection (Fig. 3). Readily detectable label representing the moving neurofilament M protein was present in 10-nm filament-free axons (Fig. 3C). Thus, tagged neurofilament M protein traveled down axons in the absence of polymer formation. In hemizygous 44A transgenic mice, although most axons lack neurofilaments (*14*), a small population with apparently normal neurofilaments is consistently encountered. In ventral roots, for example, there may be one to three fibers with neurofilaments and approximately 1000 without them. Such normal neurons apparently do not express the transgene, and consequently their axons have a normal cytoskeleton that serves as an ideal internal control. In such neurofilament polymer–positive axons, silver grains were located preferentially along or immediately adjacent to microtubules (cross-sectional view in Fig. 3D). Silver grain density was significantly higher within 50 nm of microtubules (Poisson distribution test, $P < 0.1$; $n = 101$). Longitudinal sections of vector-infected neurofilament polymer–positive axons also revealed selective channels for neurofilament transport (Fig. 3, E, F, and H). Labeled proteins tended to be situated in a line along the longitudinal axis of the axon, and this tendency became progressively more evident in the more distal portions of the labeled axons (Fig. 3, E through H). Three days after infection, the transition in the distribution pattern was observed approximately 1 mm distal from DRG neurons. At such times, the selective channels were not obvious in the vicinity of DRG neuronal cell bodies.

The results presented here suggest that neurofilament proteins can be transported in the form of monomers or small oligomers, and therefore that assembled 10-nm neurofilament polymers need not be transported by means of slow axonal transport. Our results are reenforced by observations of neurofilament L knockout mice (*22*) and of a Japanese quail line named "quiver," which has a nonsense mutation in the gene encoding neurofilament L (*23*). The phenotypes of these mutants are much alike, and both of their nerve pathologies are characterized by axonal hypotrophy associated with neurofilament polymer deficiency; yet small amounts of middle- and high-molecular-mass neurofilament proteins moved into their axons. In these animals also, the presence of intact neurofilament structures is not a prerequisite for transport of neurofilament subunits into axons.

Our investigation has several implications regarding the motors and rails used in slow axonal transport. A simple diffusion mechanism is insufficient to explain the precipitous loss of label at the wave front after the tagged protein has traveled down the axon for more than 5 mm. The fact that intra-axonal distribution of tagged protein occurs preferentially along microtubules suggests that the rails for slow axonal transport are microtubules, and therefore that the driving mechanism will be microtubule-dependent. Some members of the kinesin superfamily of proteins may serve as motors for this transport (*24*).

Because of the very dynamic equilibrium between monomers or small oligomers and neurofilament polymers that has been revealed by photobleaching studies with cultured DRG neurons (*3*), the very localized distribution of moving tagged proteins along microtubules suggests that some unknown mechanism stabilizes neurofilament proteins during transport. Neurofilament proteins on the move must be protected against Brownian movement and be slowly but effectively transported within the axon, so that the profile persists as a coherent peak weeks after labeling. Dynamic equilibrium between small oligomers and polymers involves only the portion of the protein that has been uncoupled from microtubules. Such disassociation from microtubule rails occurs behind the leading edge of transport. Our observation that the heavily labeled channels of transported neurofilament protein in neurofilament-positive axons becomes fuzzier in the proximal segments of axons may imply that incorporation into polymers has occurred in these regions.

A cell clearly does not consist of uniform protoplasm contained in a membranous bag. Rather, each structural component occupies a specific location in a highly ordered structure, and this is particularly true of neurons (*18*, *25*). We consider the slow axonal transport system to be a kind of default pathway, especially for the cytoplasmic proteins, and believe that our findings regarding neurofilament proteins will help reveal the basic mechanism underlying one of the most generalized cell biology problems: how cytosolic proteins are transported to their appropriate destinations.

REFERENCES AND NOTES

1. B. Grafstein and D. S. Forman, *Physiol. Rev.* **60**, 1167 (1980); N. Hirokawa, *Curr. Opin. Neurobiol.* **3**, 724 (1993).
2. Y. Komiya, M. Kurokawa, T. Tashiro, *Biomed. Res.* **7**, 359 (1986); R. A. Nixon and K. B. Logvinenko, *J. Cell Biol.* **102**, 647 (1986); T. Tashiro and Y. Komiya, *J. Neurosci.* **9**, 760 (1989).
3. S. Okabe, H. Miyasaka, N. Hirokawa, *J. Cell Biol.* **121**, 375 (1993); S. Takeda, S. Okabe, T. Funakoshi, N. Hirokawa, *ibid.* **127**, 173 (1994).
4. R. J. Lasek, *Philos. Trans. R. Soc. London B Biol. Sci.* **299**, 313 (1982); R. J. Lasek, J. A. Garner, S. T. Brady, *J. Cell Biol.* **99**, 212s (1984); R. J. Lasek, *J. Cell Sci. Suppl.* **5**, 161 (1986).
5. P. J. Hollenbeck, *Nature* **343**, 408 (1990); D. W. Cleveland and P. N. Hoffman, *Cell* **67**, 453 (1991); H. C. Joshi and P.W. Baas, *J. Cell Biol.* **121**, 1191 (1993).
6. S. Akli *et al.*, *Nature Genet.* **3**, 224 (1993); G. Bajocchi, S. H. Feldman, R. G. Crystal, A. Mastrangeli, *ibid.*, p. 229; B. L. Davidson, E. D. Allen, K. F. Kozarsky, J. M. Wilson, B. J. Roessler, *ibid.*, p. 219; G. Le Gal La Salle *et al.*, *Science* **259**, 988 (1993).
7. E. W. Napolitano, S. S. Chin, D. R. Colman, R. K. Liem, *J. Neurosci.* **7**, 2590 (1987).
8. G. I. Evan, G. K. Lewis, G. Ramsay, J. M. Bishop, *Mol. Cell. Biol.* **5**, 3610 (1985).
9. N. Geisler, S. Fischer, J. Vandekerckhove, U. Plessmann, K. Weber, *EMBO J.* **3**, 2701 (1984); E. Levy, R. K. Liem, P. D'Eustachio, N. J. Cowan, *Eur. J. Biochem.* **166**, 71 (1987); M. W. Myers, R. A. Lazzarini, V. M. Lee, W. W. Schlaepfer, D. L. Nelson, *EMBO J.* **6**, 1617 (1987); D. Zopf, B. Dineva, H. Betz, E. D. Gundelfinger, *Nucleic Acids Res.* **18**, 521 (1990).
10. G. Y. Ching and R. K. Liem, *J. Cell Biol.* **122**, 1323 (1993); M. K. Lee, Z. Xu, P. C. Wong, D. W. Cleveland, *ibid.*, p. 1337.
11. T. Nakagawa, J. Chen, Z. Zhang, Y. Kanai, N. Hirokawa, *ibid.* **129**, 411 (1995).
12. The recombinant adenovirus vector AxCA-NT-NFMmyc was constructed by the COS-TPC method (*26*). Briefly, an expression cosmid cassette (pAxCA-NT-NFMmyc) was constructed by insertion of the expression unit (composed of the cytomegalovirus enhancer plus the chicken β-actin promoter, a complementary DNA coding sequence, and the rabbit β-globin polyadenylation signal sequence) into Swa I site of pAxw, which is a 42-kb cosmid containing a 31-kb adenovirus type 5 genome lacking *E1A*, *E1B*, and *E3* genes. The expression cosmid cassette and the adenovirus DNA-terminal protein complex (Ad5 dlX DNA-TPC), predigested by Eco T22I, were cotransfected into 293 cells [American Type Culture Collection (ATCC); CRL1573] by calcium phosphate precipitation. The recombinant viruses were subsequently propagated with 293 cells, and the viral solution was stored at −80°C. The titers of viral stocks were determined by plaque assay on 293 cells. For in vivo injection experiments, highly concentrated recombinant viral stocks were generated by the method of Kanegae *et al.* (*15*).
13. Line 44A mice were obtained from the original breeding colony maintained at McGill University by one of the authors (A.C.P.). We chose the DRG as a site of in vivo infection because other neurons such as pyramidal neurons of the cerebral cortex and retinal ganglion cells were resistant to infection. Infection of anterior horn motor neurons, although readily achieved, might lead to the simultaneous infection of adjoining fibers of DRG neurons. Adult male and female mice of line 44A were anesthetized with ether, and dorsal root ganglia (left fourth lumbar, L4) were exposed by hemilaminectomy and were injected by means of glass needles filled with a highly concentrated (10^{10} to 10^{11} PFU/ml) recombinant adenovirus vector stock in phosphate buffered saline. Injected animals were killed between 3 and 7 days after surgery. Briefly, they were anesthetized with sodium pentobarbital and fixed by transcardiac perfusion with fresh 4% paraformaldehyde with (for immunoelectron microscopy) or without (for immunocytochemistry) 0.1% glutaraldehyde in 0.1 M phosphate buffer (pH 7.3). Immediately after perfusion, L4 dorsal roots, ganglia, and sciatic nerves were carefully excised. Consecutive 1-mm segments proceeding from the center of the DRG were removed and placed in the same fixative for an additional 2 hours at room temperature and for a further 12 hours at 4°C. The samples were then transferred to 10% sucrose in the same buffer and incubated for 2 hours at 4°C, after which they were cryoprotected with a graded series of sucrose concentrations, up to 60%, in the same phosphate buffer and then embedded in Tissue-Tek O.C.T. compound (Miles, Elkhart, IN) and frozen. For each segment, serial sections 8 to 10 μm thick were cut on a cryostat and collected. The sections were quenched (in 100 mM glycine) for 30 min at room temperature and then permeabilized and blocked (in 1% Triton X-100, 0.1% saponin, and 5% skim milk) for 4 hours at room temperature; both solutions were prepared in 0.1 M phosphate buffer (pH 7.3). Subsequently, sections were incubated overnight at 4°C with a mAb recognizing the c-Myc epitope tag (Myc 1-9E10.2 hybridoma cells; ATCC; CRL1729), followed by a second overnight incubation at 4°C with either fluorescein iso-

thiocyanate–labeled sheep anti-mouse immunoglobulin G (Amersham, Buckinghamshire, UK) for light microscopy, or with FluoroNanogold anti-mouse Fab' fluorescein (Nanoprobes, Stony Brook, NY) for electron microscopy. All antibodies were diluted in the above-mentioned permeabilizing and blocking solution. Light microscopic analysis was performed by epifluorescent light microscopy (Axiophot; Zeiss, Oberkochen, Germany) or by confocal laser scanning microscopy (MRC-1000; Bio-Rad, Cambridge, MA). For analysis of confocal laser scanning microscope images, we used CoMOS software for image collection and qualitatively oriented image processing operations and MPL software for quantitatively oriented image processing operations. The sections labeled with FluoroNanogold anti-mouse Fab' fluorescein were detected by epifluoresence microscopy, fixed again in 1% glutaraldehyde with 0.2% tannic acid in phosphate buffer, rinsed with distilled water, and subsequently processed for silver enhancement in developer [30% gum arabic, 0.85% hydroquinone, and 0.11% silver nitrate in citrate buffer (pH 7.4)]; see Hayat (*27*) for detailed procedures. After enhancement, sections were stained with 1% uranyl acetate for 2 hours at room temperature. The samples were dehydrated in a graded series of ethanol concentrations and embedded in Epon 812. Ultrathin sections were cut on a conventional ultramicrotome, stained with uranyl acetate and lead citrate, and examined with a transmission electron microscope (1200EX; JEOL, Tokyo, Japan) at an accelerating voltage of 100 KV.

14. J. Eyer and A. Peterson, *Neuron* **12**, 389 (1994).
15. Y. Kanegae, M. Makimura, I. Saito, *Jpn. J. Med. Sci. Biol.* **47**, 157 (1994).
16. M. Staufenbiel, P. Epple, W. Deppert, *J. Virol.* **60**, 1186 (1986).
17. J. J. Blum and M. C. Reed, *Cell Motil. Cytoskeleton* **12**, 53 (1989); R. A. Nixon, in *The Neuronal Cytoskeleton*, R. D. Burgoyne, Ed. (Wiley-Liss, New York, 1991).
18. N. Hirokawa, *J. Cell Biol.* **94**, 129 (1982).
19. Virus-injected animals (*13*) were killed 2 days after infection; both proximal and distal nerve fragments from injected ganglia, each 2 mm in length, were isolated and homogenized in 100 μl PEM [100 mM Pipes (pH 6.9), 1 mM EGTA, 1 mM $MgCl_2$, 1 mM dithiothreitol, 1 mM phenylmethylsulfonyl fluoride, and leupeptin (100 μg/ml)] with 1% Triton X-100. Homogenates were resolved on a 7.5% SDS-polyacrylamide gel, electrotransferred onto a polyvinylidene difluoride membrane (Immobilon PVDF; Millipore, Bedford, MA), and probed with mAb to c-Myc and mAb to neurofilament M (NN18; BioMakor, Rehovot, Israel). The bound antibodies were detected with ^{125}I-labeled protein A (Amersham) and analyzed with an image analyzer (BAS 2000; Fuji, Tokyo, Japan).
20. S. Terada, T. Nakata, A. C. Peterson, N. Hirokawa, data not shown.
21. J. F. Engelhardt, X. Ye, B. Doranz, J. M. Wilson, *Proc. Natl. Acad. Sci. U.S.A.* **91**, 6196 (1994); B. R. Grubb *et al.*, *Nature* **371**, 802 (1994); Y. Yang *et al.*, *Nature Genet.* **7**, 362 (1994); Y. Yang *et al.*, *Proc. Natl. Acad. Sci. U.S.A.* **91**, 4407 (1994).
22. J.-P. Julien *et al.*, unpublished data.
23. H. Yamasaki, G. S. Bennett, C. Itakura, M. Mizutani, *Lab. Invest.* **66**, 734 (1992); O. Ohara, Y. Gahara, T. Miyake, H. Teraoka, T. Kitamura, *J. Cell Biol.* **121**, 387 (1993).
24. N. Hirokawa, *Trends Cell Biol.* **6**, 135 (1996).
25. ———, G. S. Bloom, R. B. Vallee, *J. Cell Biol.* **101**, 227 (1985).
26. I. Saito, Y. Oya, K. Yamamoto, T. Yuasa, H. Shimojo, *J. Virol.* **54**, 711 (1985); Y. Kanegae *et al.*, *Nucleic Acids Res.* **23**, 3816 (1995); S. Miyake *et al.*, *Proc. Natl. Acad. Sci. U.S.A.* **93**, 1320 (1996).
27. M. A. Hayat, *Principles and Techniques of Electron Microscopy* (CRC Press, Boca Raton, FL, 1989).
28. We thank I. Saito and Y. Kanegae (Institute of Medical Science, University of Tokyo) and J. Miyazaki (University of Tokyo School of Medicine) for supplying us with their recombinant adenovirus vector system and the CAG promoter, respectively. Their technical advice was essential for the successful construction of our vector. We also thank Y. Komiya and T. Tashiro (Gunma University School of Medicine) for their technical assistance and advice on the microinjection into dorsal root ganglia in vivo; S. Ijuin (Nippon Bio-Rad Laboratories) for his technical assistance in confocal laser scanning microscopy; H. Yorifuji (National Defense Medical College) for his guidance in electron microscopic procedures; J.-P. Julien (Montreal General Hospital Research Institute, Centre for Research in Neuroscience, McGill University) and R. Nixon (McLean Hospital, Harvard Medical School) for helpful comments on the manuscript and useful discussions; Y. Kobayashi (Kyorin University School of Medicine) and T. Funakoshi, S. Kondo, Y. Okada, and other members of the Hirokawa lab for stimulating discussions and invaluable advice throughout; and Y. Kawasaki, H. Sato, H. Fukuda, and Y. Sugaya for their technical and secretarial assistance. Supported by a Special Grant-in-Aid for Scientific Research from the Japan Ministry of Education, Science and Culture; a grant from the Institute of Physical and Chemical Research (RIKEN) to N.H.; a Grant-in-Aid for Scientific Research from the Japan Ministry of Education, Science and Culture to S.T.; and grants from the Medical Research Council of Canada and Muscular Dystrophy Association of Canada to A.C.P.

22 April 1996; accepted 10 June 1996

Immunodeficiency in Protein Kinase Cβ–Deficient Mice

Michael Leitges,*†‡ Christian Schmedt,* Rodolphe Guinamard, Jean Davoust, Stefan Schaal, Silvia Stabel, Alexander Tarakhovsky†

Cross-linking of the antigen receptor on lymphocytes by antigens or antibodies to the receptor results in activation of enzymes of the protein kinase C (PKC) family. Mice homozygous for a targeted disruption of the gene encoding the PKC-βI and PKC-βII isoforms develop an immunodeficiency characterized by impaired humoral immune responses and reduced cellular responses of B cells, which is similar to X-linked immunodeficiency in mice. Thus PKC-βI and PKC-βII play an important role in B cell activation and may be functionally linked to Bruton's tyrosine kinase in antigen receptor–mediated signal transduction.

Cross-linking of the antigen receptor on B and T cells by antigens or by antibodies to the receptor is accompanied by rapid phospholipase C–γ activation, resulting in phospholipid hydrolysis and subsequent activation of the serine-threonine–specific protein kinase C (PKC) (*1*). The term PKC defines a family of at least 10 proteins that are characterized by a high degree of homology in their catalytical and cysteine-rich domains. On the basis of structural similarity and the requirement of Ca^{++} or diacylglycerol (DAG) or both for catalytic activity, the PKC family has been subdivided into three groups. The Ca^{++}- and DAG-dependent PKCs are represented by PKC-α, -βI, -βII, and -γ isoforms; PKC-δ, -ϵ, -η, and -θ are DAG-dependent but Ca^{++}-independent; and PKC-ζ and -λ are not activated by Ca^{++} and DAG in vitro (*2*). Despite extensive information on the enzymatic properties and expression patterns of various PKC isoforms in cells of the hematopoetic system, little is known about the physiological role of individual PKC isoforms in lymphocyte function (*3*). We started to address this question with the analysis of the immune system of mice deficient for the Ca^{++}-DAG–dependent PKC-βI and -βII. Both PKC-β isoforms are encoded by the same gene and are expressed in B and T lineage cells (*4*).

The gene encoding PKC-β was disrupted in embryonic stem (ES) cells by insertion of a *lacZ-neo* cassette into the second exon of the PKC-β gene by homologous recombination (Fig. 1) (*5*). The presence of the targeted PKC-β allele in mice heterozygous or homozygous for the mutation was revealed by Southern (DNA) blot analysis (Fig. 1B). The absence of PKC-β protein in homozygous mutant mice was confirmed by protein immunoblot analysis of lysates of splenocytes and thymocytes (Fig. 1C) (*5*).

Analysis of lymphocyte populations revealed that the frequency and absolute number of the $CD23^-$ immunoglobulin M^+ (IgM^+) (B-1) B lymphocytes as well as of $CD5^+$ IgM^+ (B-1a) cells, which represent a substantial fraction of the B-1 lymphocyte population, were severely reduced in the peritoneal cavity of PKC-$\beta^{-/-}$ mice as compared with that of wild-type mice (Fig. 2) (*6*). B-1 lymphocytes are located predominantly in the peritoneal cavity of mice and are thought to belong to a separate B cell lineage that differs from those of other B

M. Leitges and S. Stabel, Max-Delbrück-Laboratorium in der Max-Planck-Gesellschaft, Carl-von-Linné-Weg 10, D-50829 Köln, Germany.
C. Schmedt, S. Schaal, A. Tarakhovsky, Institute for Genetics, University of Köln, Weyertal 121, D-50931 Köln, Germany.
R. Guinamard and J. Davoust, Centre d'Immunologie CNRS-INSERM de Marseille-Luminy, Case 906, 13288 Marseille Cedex 9, France.

*These authors contributed equally to this work.
†To whom correspondence should be addressed.
‡Present address: Max-Planck-Institut für Immunbiologie, Stübeweg 51, D-79108 Freiburg, Germany.